Universal Length Dependence of Rod-to-Seed Exciton Localization Efficiency in Type I and Quasi-Type II CdSe@CdS Nanorods

Kaifeng Wu,[†] Lawrence J. Hill,[‡] Jinquan Chen,[†] James R. McBride,[§] Nicholas G. Pavlopolous,[‡] Nathaniel E. Richey,[‡] Jeffrey Pyun,[*,‡,⊥] and Tianquan Lian[*,†]

[†]Department of Chemistry, Emory University, 1515 Dickey Drive, NE, Atlanta, Georgia 30322, United States, [‡]Department of Chemistry and Biochemistry, University of Arizona, 1306 East University Boulevard, Tucson, Arizona 85721, United States, [§]Department of Chemistry, The Vanderbilt Institute of Nanoscale Science and Engineering, Vanderbilt University, Nashville, Tennessee 37235, United States, and [⊥]School of Chemical & Biological Engineering, Seoul National University, Seoul 151-744, Republic of Korea

ABSTRACT A critical step involved in many applications of one-dimensional seeded CdSe@CdS nanorods, such as luminescent solar concentrators, optical gains, and photocatalysis, is the localization of excitons from the light-harvesting CdS nanorod antenna into the light-emitting CdSe quantum dot seed. We report that the rod-to-seed exciton localization efficiency decreases with the rod length but is independent of band alignment between the CdSe seed and CdS rod. This universal dependence can be well modeled by the competition between exciton one-dimensional diffusion to the CdSe seed and trapping on the CdS rod. This finding provides a rational approach for optimizing these materials for their various device applications.

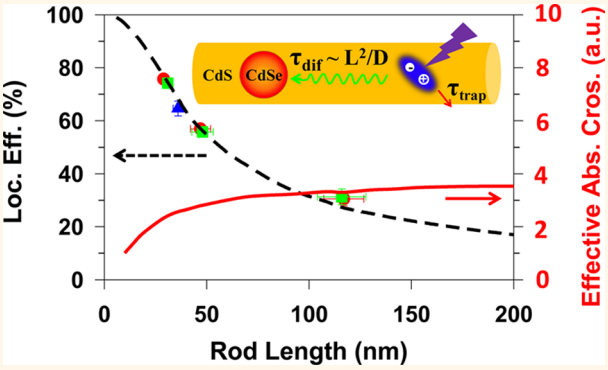

KEYWORDS: nanoheterostructure · CdSe@CdS · nanorods · exciton localization · exciton diffusion · luminescent solar concentrator

Compared to zero-dimensional (0D) quantum dots (QDs), colloidal one-dimensional (1D) quantum confined semiconductor nanostructures, such as nanorods (NRs) and tetrapods,[1−4] have larger absorption cross sections,[5−7] enhanced stabilities,[8,9] longer multiexciton lifetimes,[10−13] and linearly polarized emissions,[14−19] making them promising light-harvesting, light-emitting, and photocatalysis materials.[11,20−29] Among them, 1D NR heterostructures consisting of multiple components can lead to properties that cannot be achieved in single-component materials.[2,4,30−35] CdSe@CdS dot-in-rod NRs (CdSe@CdS hereafter for simplicity), with a CdS NR grown from a CdSe QD seed, is one of the most intensely studied 1D heterostructures.[15,16,29,36−41] Due to the large valence band (VB) offset (>0.45 eV) and small conduction band (CB) offset (<0.3 eV) between bulk wurtzite CdSe and CdS,[15,38] the band alignment of these CdSe@CdS NRs can be tuned by the seed size and rod diameter from type I (with the lowest energy electron and hole levels confined in the CdSe seed) to quasi-type II (with the lowest energy hole confined in the CdSe seed and the lowest energy electron level degenerate in CdSe and CdS).[37−48] While it is clear that in type I NRs the lowest energy exciton is confined in the CdSe seed, extensive recent studies have revealed that in quasi-type II NRs, the electron in the lowest energy exciton state is also localized at and near the CdSe seed,[41,42,49] due to strong electron−hole bindings in 1D nanostructures.[50] Therefore, in these heterostructures, the CdS rods acts as nanoscale light-harvesting antennas and the photogenerated excitons in the rod can be transported and localized to the CdSe seed,[40] mimicking natural light-harvesting complexes.[51,52] For this reason, CdSe@CdS NRs have been applied to solar-to-fuel conversion,[23,27,53] luminescent solar

* Address correspondence to tlian@emory.edu, jpyun@email.arizona.edu.

Received for review February 25, 2015 and accepted March 24, 2015.

Published online March 24, 2015
10.1021/acsnano.5b01245

concentrators,[54] and optical gains.[28,29,55] These applications all take advantage of the large volume of CdS rods for efficient light absorption and funnel photogenerated excitons into CdSe seeds, where chemical reactions or light emissions occur.

Exciton transport from the CdS rod to the CdSe seed in CdSe@CdS NRs involves not only energy relaxation from higher to lower energy exciton states but also charge transport over a length scale of 10−1000 nm. Such long-distance exciton transport is susceptible to energetic disorder along the length of the rod caused by diameter variations and trap states.[40] It has been reported that the rod-to-seed exciton localization efficiency is not unity, and there exist long-lived excitons trapped on the CdS rod in addition to localized excitons at the CdSe seed.[46,56,57] But it remains unclear how these excitons are transported along the rods and how the branching ratio of the aforementioned pathways depends on the length of the rods and the seed/rod band alignment. In this paper, we report a study of the rod length dependence of exciton localization efficiency in CdSe@CdS NRs with both type I and quasi-type II band alignments. By photoluminescence excitation (PLE) spectroscopy and transient absorption (TA) spectroscopy, we observed that the exciton localization efficiency was independent of the band alignment but decreased at longer rod length. We showed that this universal length dependence could be accounted for by the competition between 1D exciton diffusion from the rod to the seed and exciton trapping at the rod. We believe that the proposed model is generally applicable to other 1D nanoheterostructures, providing guidance for a rational design of NR morphology for their many applications.

Preparation and Morphological Characterization of CdSe@CdS NRs. CdSe@CdS NRs of varying dimensions were synthesized using modified approaches from the method of Manna and co-workers,[16,37,58,59] where CdSe QDs of different sizes were used as seeds to prepare CdS NRs. Synthetic details can be found in the Methods section and Supporting Information (SI). An attractive feature of these heterostructures is the ability to prepare NRs of uniform length and diameter by controlling the ratio of CdSe QD seeds to CdS NR precursors (SI). In the current report, seven NR samples were prepared using three CdSe seed sizes (diameter = 2.5, 2.7, and 3.8 nm): three NRs of different lengths were grown with 2.7 and 3.8 nm CdSe seeds, and one NR was grown for 2.5 nm seeds. For convenience we labeled them by their seed diameters and rod lengths. For example, $CdSe_{2.5}@CdS_{36}$ has a seed diameter of 2.5 nm and rod length of 36 nm. Representative transmission electron microscopy (TEM) images of NRs grown from 2.7 and 3.8 nm seeds are shown in column 1 of Figure 1 and Figure 2, respectively. These seeded NRs exhibited relatively uniform diameters

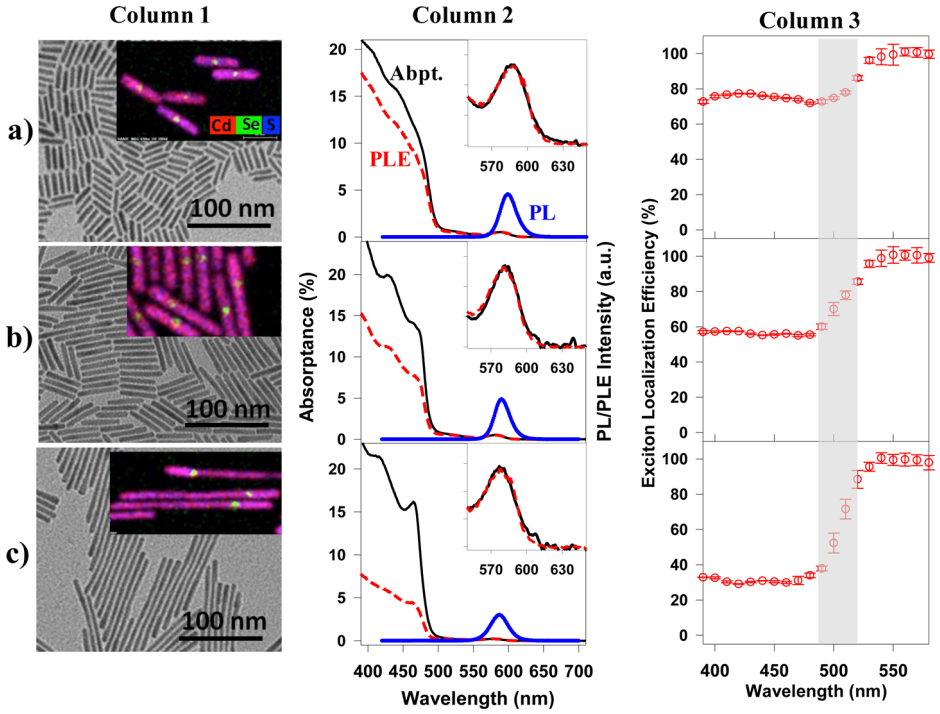

Figure 1. Quasi-type II CdSe@CdS NRs (2.7 nm seed). (Column 1) Representative TEM images, (column 2) absorptance (black solid line), photoluminescence (PL, blue solid line), and photoluminescence excitation (PLE, red dashed line) spectra, and (column 3) wavelength-dependent relative PL QYs of (a) $CdSe_{2.7}@CdS_{29}$, (b) $CdSe_{2.7}@CdS_{47}$, and (c) $CdSe_{2.7}@CdS_{117}$ NRs. Column 1 insets: color-coded EDX elemental maps of Se (green, indicating location of the CdSe seed), Cd (red), and S (blue). Note that they are arbitrarily enlarged and do not share the same scale bar as the TEM images. The PLE and absorptance spectra in column 2 have been normalized at the lowest energy exciton peak (an expanded view is shown in the insets). The shaded areas in column 3: regions of gradual decrease of relative PL QYs.

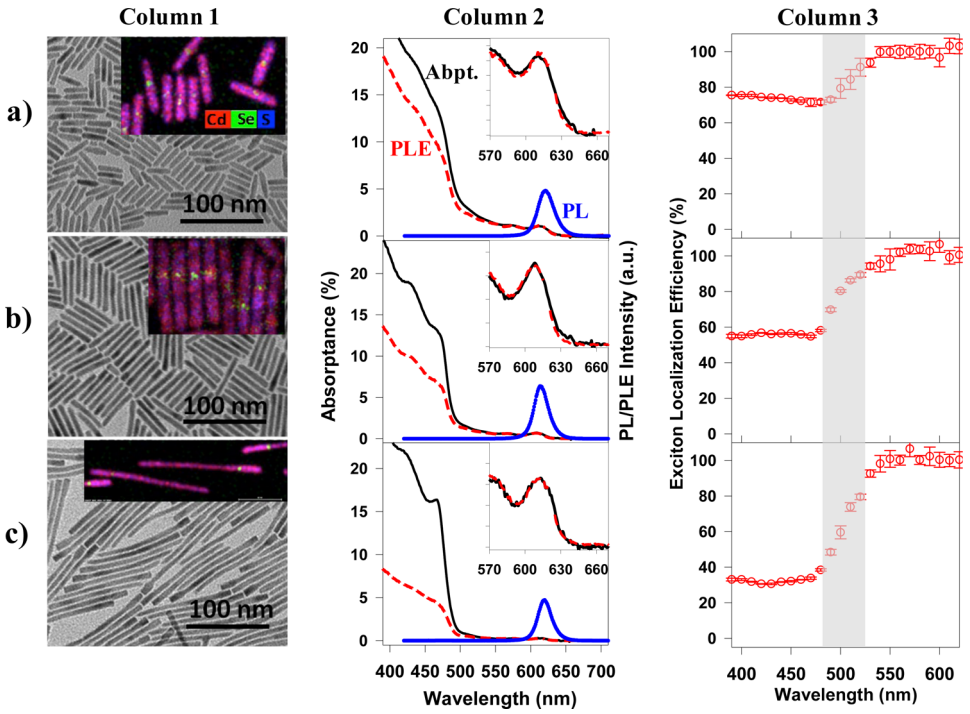

Figure 2. Type-I CdSe@CdS NRs (3.8 nm seed). (Column 1) Representative TEM images, (column 2) absorptance (black solid line), photoluminescence (PL, blue solid line), and photoluminescence excitation (PLE, red dashed line) spectra, and (column 3) wavelength-dependent relative PL QYs of (a) $CdSe_{3.8}@CdS_{31}$, (b) $CdSe_{3.8}@CdS_{48}$, and (c) $CdSe_{3.8}@CdS_{116}$ NRs. Column 1 insets: colored-coded EDX elemental maps of Se (green, indicating location of CdSe seed), Cd (red), and S (blue). Note that they are arbitrarily enlarged and do not share the same scale bar as the TEM images. The PLE and absorptance spectra in column 2 have been normalized at the lowest energy exciton peak (an expanded view is shown in the insets). The shaded areas in column 3: regions of gradual decrease of relative PL QYs.

without the incidence of geometric or morphological defects along the 1D CdS phase (see SI Figures S1−S4 and Table S1 for NR dimensional analysis).[36,40] In addition, we observed that increasing rod length was accompanied by a slight decrease in the average rod diameter (Table S1) from 5.6 ± 0.7 nm in $CdSe_{2.7}@CdS_{29}$ to 4.9 ± 0.6 nm in CdSe2.7@CdS_{117}. Similarly, for a 3.8 nm seed, the average rod diameter decreased from 5.9 ± 0.6 nm in $CdSe_{3.8}@CdS_{31}$ to 4.8 ± 0.7 nm in $CdSe_{3.8}@CdS_{116}$. In general, the morphology of these nanorods can be approximately represented by a uniform CdS nanorod with an enclosed CdSe seed as depicted in Scheme 1a.

Energy-dispersive X-ray spectroscopy (EDX) was used to analyze the element distribution along the NRs and to identify the position of the CdSe seed for the series of NRs investigated in this study. These seed positions are crucial when determining rod-to-seed exciton transport distances. As shown in the insets of column 1 of Figure 1, the CdSe seeds can be traced by the green Se regions, from which average seed positions were determined (Table S2). Roughly, the seeds were located at ~1/2, 1/3, and 1/5 of the total rod lengths of $CdSe_{2.7}@CdS_{29}$, $CdSe_{2.7}@CdS_{47}$, and $CdSe_{2.7}@CdS_{117}$, respectively. Similar trends were observed for NRs with 2.5 nm (see SI, Figure S2) and 3.8 nm seeds (column 1, Figure 2). It has often been assumed that the seed is located at 1/4 of the rod

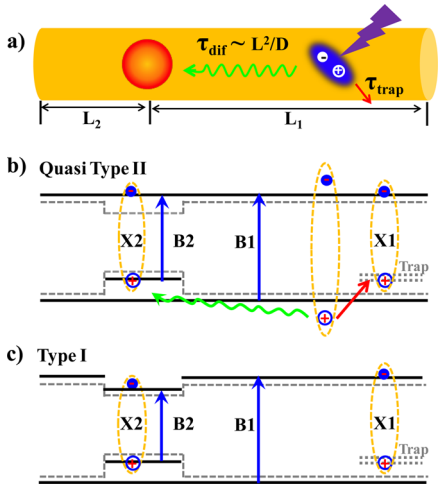

Scheme 1. Electronic structure and exciton dynamics in type I and quasi-type II CdSe@CdS NRs. (a) Schematic illustration of a CdSe@CdS seeded NR and the relaxation processes (localizing to the CdSe seed or trapping at the CdS rod) of an exciton generated at the CdS rod. Schematic energy level diagrams of (b) quasi-type II (2.7 and 2.5 nm seeds) and (c) type I (3.8 nm seeds) CdSe@CdS NRs, showing bulk band edges of CdS and CdSe (gray dotted lines) and lowest electron and hole energy levels in the CdSe seed and the CdS rod (black solid lines) and sub-band gap hole trapping states on the CdS rod (black dotted lines). Also labeled are excitons trapped on the CdS rod (X1) and localized at the CdSe seed (X2) as well as lowest energy transitions in the CdS rod (B1) and the CdSe seed (B2).

length due to different growth rates of the two terminating facets of CdS NRs.[16,37] Our result indicates that the seed is close to the center of short rods but deviates gradually from the center for longer rods. The detailed morphological parameters (including seed size, seed position, rod length, and rod diameter) for all investigated NRs are summarized in Table S1.

Electronic Structure of Type I and Quasi-Type II CdSe@CdS NRs. The optical absorption and emission spectra of these NRs confirmed that the band alignment of CdSe and CdS can be tuned from type I to quasi-type II by decreasing the CdSe seed sizes. The absorption spectra of all NRs are shown in Figure S7. The absorptance, photoluminescence (PL), and photoluminescence excitation (PLE) spectra of NRs with 2.7 and 3.8 nm seeds and different lengths are shown in column 2 of Figure 1 and Figure 2, respectively. For a better comparison with PLE spectra (PL intensity as a function of excitation wavelength), we have shown the absorptance spectra (absorptance = $1-10^{-OD}$, where OD is optical density, representing the percentages of absorbed photons as a function of wavelength) instead of the absorption spectra in Figures 1 and 2. Extensive studies of related CdSe@CdS NRs have shown that their electronic structure can be described by the schematic energy level diagrams depicted in Scheme 1b and c.[37,39,40,44,46,47,56,57] Because of the large valence band and small conduction band offsets between CdSe and CdS, CdSe@CdS NRs can exhibit band alignments of either quasi-type II for small CdSe seeds[37] (Scheme 1b) or type I for large CdSe seeds[38] (Scheme 1c) depending on the extent of quantum confinement in the seed.[39] Quantum confinement in the radial direction leads to discrete electron and hole energy levels in the CdS rod, and excitonic transitions between these levels give rise to the 1D exciton bands at <480 nm in the absorption spectra.[37,56] As shown in column 2 of Figure 1 and Figure 2 (and Figure S7), the absorption bands at ~475 and 420 nm can be attributed to the lowest energy 1Σ (or B1) and 1Π excitonic bands of CdS rods, respectively. In addition, the absorption spectra showed excitonic features of >512 nm (smaller than the CdS bulk band gap of 2.42 eV[60]) that can be associated with transitions from the CdSe seed. The transition energies of CdSe features depended sensitively on the size of CdSe seeds, with the lowest excitonic band at ~580 and ~610 nm for NRs with 2.7 and 3.8 nm seeds, respectively. We labeled this transition as B2 in Scheme 1b and c. With increasing rod length, the relative amplitude of the CdS absorption (B1) became larger because of its increasing volume. For both NRs with the 2.7 and 3.8 nm seed, the B1 exciton peak positions were blue-shifted with increasing rod length (Figure S7), reflecting decreasing diameters at longer rod lengths. Interestingly, the same length dependence was observed in the B2 transition for NRs with a 2.7 nm seed, but not for NRs with a 3.8 nm seed (Figure S7 and Table S2). This result

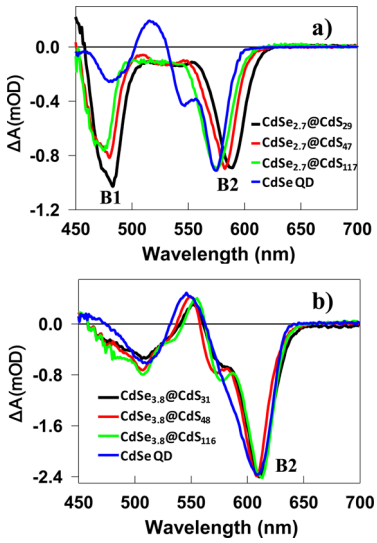

Figure 3. Averaged transient absorption (TA) spectra of NRs with a 2.7 nm (a) and 3.8 nm (b) seed measured at 1−2 ps after 575 nm excitation. For comparison, TA spectra of corresponding CdSe QDs with similar confinement energies are also shown.

suggests that the B2 transition energy of NRs with a 2.7 nm seed is sensitive to the energy level of the CdS rod, consistent with a quasi-type II band alignment (Scheme 1b), and the B2 transition energy of NRs with a 3.8 nm seed is insensitive to the energy level of the CdS rod, exhibiting a type I band alignment (Scheme 1c).

To further confirm the band alignment in these NRs, we carried out a transient absorption study following previous works.[37,56,61] In these measurements, we selectively excited these samples at 575 nm, the lowest energy transition (B2), to generate an X2 exciton (see Scheme 1b and c) in the seed. The resulting TA spectra (averaged between 1 and 2 ps delay) for NRs with 2.7 and 3.8 nm seeds are shown in Figure 3a and b, respectively. Their kinetics in Figure S9 show that these spectral features form instantaneously (<10 fs) and only slightly decay (<15%) within 1 ns, indicating dominant single-exciton conditions.[29] For NRs with a 2.7 nm seed (Figure 3a), 575 nm excitation led to a strong bleach of both the B2 band of the CdSe seed (~580 nm) and the B1 band of the CdS rod (~475 nm). Since these bleaches are caused by the state filling of the CB electron level,[56] the instantaneous formation of both B1 and B2 bleaches indicates that the electron wave function of the X2 exciton extends from the CdSe seed into the CdS rod, consistent with a quasi-type II electronic structure (Scheme 1b).[41,56] A similar electron wave function delocalization and quasi-type II band alignment was observed for the $CdSe_{2.5}@CdS_{36}$ NR (Figure S10). In contrast, for NRs with a 3.8 nm seed (Figure 3b), 575 nm excitation led to a strong B2 bleach and negligible B1 bleach, indicating that the electron wave function of the X2 exciton has negligible amplitude at the CdS rod, consistent with a type I electronic structure (Scheme 1c). There exists a derivative-like

feature near B1 (Figure 3b), which is also observed in CdSe QDs of similar confinement energy (Figure 3b) and can be attributed to the effect of the lowest energy exciton on the higher energy transitions (i.e., biexciton interaction) of the CdSe seed.[62]

Length-Dependent Exciton Localization Efficiency. PL spectra of all NRs studied in this work (column 2 of Figure 1 and 2 and Figure S8c) showed pronounced X2 exciton emission that was slightly red-shifted from the B2 absorption band of the seed and negligible emission from the CdS rod, consistent with previous reports.[16,36] PLE spectra shown in Figures 1 and 2 were acquired by monitoring the emission at the PL peak (with a detection bandwidth of 2 nm) and have been normalized to the same amplitude as the absorptance spectra at the B2 band. The ratio of normalized PLE over absorptance yields relative PL quantum yields (QYs), which is also the efficiency of converting (localizing) the initial photogenerated exciton on the rod to the X2 exciton in the seed (with the localization efficiency for excitation at the B2 band set to 1).[56] As shown in column 3 of Figures 1 and 2, for all these NRs, the exciton localization efficiencies were constant (unity) at wavelengths longer than 520 nm where light absorption occurs at the CdSe seed, decreased gradually at 480−520 nm when the absorption of CdS rods increased, and leveled off at wavelengths shorter than 480 nm to ~75.7 ± 1.5% (74.2 ± 1.2%), 55.9 ± 1.6% (55.8 ± 0.7%), and 30.5 ± 2.6% (31.3 ± 3.0%) for $CdSe_{2.7}@CdS_{29}$ ($CdSe_{3.8}@CdS_{31}$), $CdSe_{2.7}@CdS_{47}$ ($CdSe_{3.8}@CdS_{48}$), and $CdSe_{2.7}@CdS_{117}$ ($CdSe_{3.8}@CdS_{116}$), respectively. At < 480 nm (above the CdS rod band gap), the absorption is dominated by CdS rods due to their much larger volume than CdSe seeds and the measured exciton localization efficiency reflects the localization of excitons generated at the CdS rod to (near) CdSe seed in these NRs, driven by the large VB offset (>0.45 eV).[53,56] Similar measurements were performed on the $CdSe_{2.5}CdS_{36}$ sample, and the rod-to-seed exciton localization efficiency was determined to be 64.6 ± 2.8% (Figure S8). These results, plotted in Figure 4, showed that the rod-to-seed exciton localization efficiency for these NRs was independent of the seed size but decreased with rod length. Since the NRs with 2.5 and 2.7 nm seeds have quasi-type II band alignments different from the type I band alignment in NRs with 3.8 nm seeds, the seed size independence indicates that the band alignment does not affect the exciton localization process in these NRs.

Exciton Trapping on Nanorods. The observed nonunity rod-to-seed exciton localization efficiencies and their rod length dependence suggest the presence of other exciton localization pathways that compete with exciton transport to the CdSe seed. Through studies of related CdSe@CdS NRs and CdS NRs, we have previously attributed this competition process to hole-trapping-induced exciton localization on CdS NRs.[56]

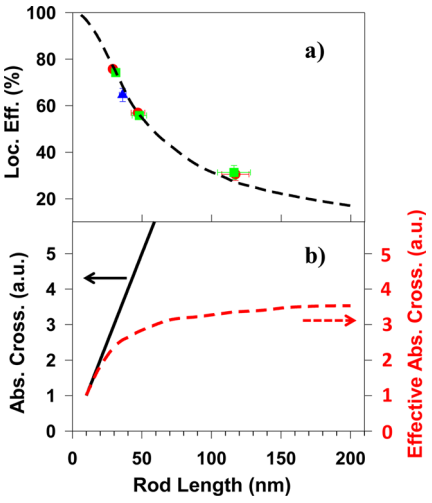

Figure 4. Universal length dependence of exciton localization. (a) Measured (symbols) and simulated (dashed line) exciton localization efficiencies in CdSe@CdS NRs with 2.5 nm (blue triangles), 2.7 nm (red circles), and 3.8 nm (green squares) seeds. (b) CdS rod absorption cross-section (black solid line) and effective CdSe seed absorption cross-section (red dashed line) as a function of rod length.

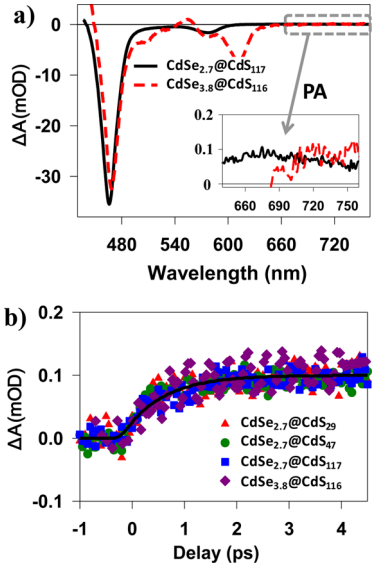

Figure 5. (a) TA spectra of $CdSe_{2.7}@CdS_{117}$ (black solid line) and $CdSe_{3.8}@CdS_{116}$ (red dashed line) averaged between 5 and 10 ps after 400 nm excitation. The inset is the expanded view of the photoinduced absorption (PA) signal from 640 to 760 nm. (b) Formation kinetics of the PA signal for $CdSe_{2.7}@CdS_{29}$ (red triangles), $CdSe_{2.7}@CdS_{47}$ (green circles), $CdSe_{2.7}@CdS_{117}$ (blue squares), and $CdSe_{3.8}@CdS_{116}$ (purple diamonds). The black solid line is a fit using single-exponential formation.

Although the hole trapping time constant was reported to be ~0.7 ps for CdS NRs with an average length of 29 nm,[63] the length dependence of this process remains unknown. To this end, we have measured the hole trapping time for NRs used in this study by TA spectroscopy. Representative average TA spectra at 5−10 ps after 400 nm excitation for $CdSe_{2.7}@CdS_{117}$ and $CdSe_{3.8}@CdS_{116}$ are shown in Figure 5a. These

spectra exhibited a small and broad photoinduced absorption (PA) signature at wavelengths longer than the B2 exciton band, which has been assigned to trapped holes on the surfaces of CdS rods (by selective removal of electrons from the rods in the presence of electron acceptors).[63] Comparison of NRs with 2.7 and 3.8 nm seeds of different lengths (Figure 5b) showed that the formation kinetics of the PA signal was independent of the rod length or seed size. Single-exponential fit to these kinetics revealed a hole trapping time of $\tau_{Trap} = 0.78 \pm 0.13$ ps, similar to our previous result of CdS NRs.[63] Although the reason for the lack of length dependence in the hole trapping rate is unclear, it may indicate that the hole trap density is independent of rod length. We speculate that they are likely associated with defects on the rod surfaces, such as the unpassivated sulfur anions,[64] that increase proportionally with the rod length.

Mechanism of Universal Length-Dependent Exciton Localization Efficiency. In the following, we consider three possible mechanisms of exciton localization from the CdS rod to the CdSe seed: energy transfer, ballistic exciton transport, and exciton diffusion.[65] These mechanisms can be differentiated by their dependence on the rod length. The energy transfer time constant is proportional to the sixth power of the donor−acceptor distance according to the Forster resonant energy transfer (FRET) theory.[66] Therefore, the length dependence of the energy transfer rate can be readily calculated, even though reliable estimates of the absolute energy transfer rate, requiring the information on absorption and emission cross sections, are difficult for these NRs. The simulated results in Figure S11 showed that the FRET mechanism led to a much stronger distance dependence of the exciton localization efficiency than the measured trend shown in Figure 4. Further details of the simulation can be found in the SI.

Ballistic transport occurs within the carrier mean free path (L_{mfp}). L_{mfp} in CdS NRs is related to the product of the scattering time constant, τ_c, and thermal velocity at room temperature (RT), v_{th}, through $L_{mfp} \approx \tau_c v_{th}$.[67] τ_c can be calculated from the reported carrier mobility (μ) through $\tau_c = \mu m^*/q$,[67] where m^* and q are the effective mass and charge of the particle, respectively. The reported upper limit of electron (hole) mobility in bulk single crystal CdS at room temperature is ~400 (~48) $cm^2\ s^{-1}\ V^{-1}$,[68−72] which corresponds to an upper limit of the mean free path of ~4 (1.6) nm. Exciton mean free path should be limited by holes and also has a upper limit of ~1.6 nm in CdS NRs. The short carrier mean free path in CdS has been attributed to their strong interactions with phonons, through Frohlich, deformation potential, or piezoelectric scatterings.[73] Therefore, in our NRs with lengths of 10's to 100's of nanometers, exciton and carrier transport should proceed through diffusion.

We then model the exciton localization process by accounting for the competition between exciton diffusion and exciton trapping. As shown in Scheme 1a, the CdSe seed divides the CdS NR into two segments with lengths of L_1 and L_2. We solve the exciton localization problem within L_1 and L_2 using the modified 1D diffusion equation:

$$\frac{\partial N(x,t)}{\partial t} = D\frac{\partial^2 N(x,t)}{\partial^2 x} - \frac{N(x,t)}{\tau_{Trap}} \quad (1)$$

where D is the exciton diffusion constant and $N(x,t)$ is the concentration of excitons at a distance x from the seed at time t. The second part on the right-hand side of eq 1 accounts for depopulation of the CdS band edge excitons due to trapping. The boundary conditions for this equation are $N(x,t=0) = N_0$, $N(x=0,t) = 0$, and $J(x=L_{1(2)},t) = [\partial N(x=L_{1(2)},t)]/\partial x = 0$. The first boundary condition indicates randomly generated excitons along the rod; the second one assumes that exciton transfer across the CdS/CdSe interface (*i*.e., capture by the CdSe seed) is much faster than the diffusion process within the CdS rod; the third one indicates that the fluxes crossing the NR ends are zero. Using these boundary conditions, eq 1 is analytically solvable and the details are shown in the SI. With the solution of $N(x,t)$, the ensemble-averaged exciton population on the rod, $S(t)$, is obtained by integrating $N(x,t)$ over the rod length:

$$S_{L_1}(t) \propto \int_0^{L_1} N(x,t)\,dx \propto \sum_{n=1}^{\infty}\frac{1}{n^2} e^{-\left[D\left(\frac{n\pi}{2L_1}\right)^2 + \frac{1}{\tau_{Trap}}\right]t} \quad (2)$$

where n is an odd integer 1, 3, 5, ... The exponent in eq 2 reflects the competition between carrier trapping, with a time constant of τ_{Trap}, and diffusion, whose characteristic time scale is proportional to the square of the diffusion length.[74] The efficiency of exciton localization to the seed within L_1 is calculated as

$$\Phi(L_1) = \sum_{n=1}^{\infty}\frac{1}{n^2}\frac{D\left(\frac{n\pi}{2L_1}\right)^2}{D\left(\frac{n\pi}{2L_1}\right)^2 + \frac{1}{\tau_{Trap}}} \Big/ \sum_{n=1}^{\infty}\frac{1}{n^2} \quad (3)$$

$\Phi(L_2)$ can be calculated in the same way, and the overall localization efficiency $\Phi(L)$ is obtained by the length-weighted average of $\Phi(L_1)$ and $\Phi(L_2)$:

$$\Phi(L) = \frac{L_1\Phi(L_1) + L_2\Phi(L_2)}{L_1 + L_2} \quad (4)$$

With the exciton diffusion constant D as the only fitting parameter, we simultaneously fit the localization efficiency for all NRs, as shown in Figure 4a. From the best fit, we obtained a diffusion constant D of 2.3×10^{-4} m^2/s. The electron (D_e) and hole (D_h) diffusion constants in bulk CdS, calculated from their mobilities, are $\sim 10 \times 10^{-4}$ and 1.2×10^{-4} m^2/s, respectively.

The exciton center of mass diffusion constant (D_X) can be calculated to be 3.2×10^{-4} m^2/s. Our fitted exciton diffusion constant in CdS NRs is slightly smaller than the bulk value, which is reasonable considering additional scattering channels due to the presence of large surface areas in NRs.[75] Our simulation result confirms that the rod-to-seed exciton localization efficiency is controlled by the competition between exciton diffusion and exciton trapping, which is independent of the rod/seed band alignment, and is dependent on the rod length in a predictable manner.

Implications for Device Performance. CdSe@CdS NRs have been used as light-absorbing materials in luminescent solar concentrators in which the large CdS rod absorption, efficient rod-to-seed exciton localization, and small CdSe seed reabsorption loss enable the concentration of absorbed solar flux by the rod into the emission at the seed.[54] Although the requirement of large rod absorption and small seed reabsorption can be realized by increasing the rod length, there exists an optimal rod length because the rod-to-seed localization efficiency decreases at longer rod length. Thus, it is useful to define an effective light-harvesting power (or effective absorption cross section) for these CdSe@CdS NRs as a product of the absorption cross section of the rod and the rod-to-seed exciton localization efficiency. This quantity represents the effective cross section for creating excitons in the seed through absorption at the rod. The fit to the measured data discussed above gives a prediction of exciton localization efficiencies of all NRs in the length ranges of 10 to 200 nm, as shown in Figure 4a. In this calculation, we have assumed that the seed positions followed the trend observed for the NRs we studied (Figure S12; see SI for details), and the absorption cross section of the rod increases linearly with the rod length. The calculated effective seed absorption cross section (Figure 4b) initially increases with the rod length and levels off at a rod length of ~100 nm. In this calculation, we have set the cross sections to one for NRs of 10 nm in length. The effective seed absorption cross section levels off at a value that is 3.5 times that of a 10 nm rod, despite a factor of 10 and higher total absorption cross section of the CdS rod at a rod length exceeding 100 nm. Further increase in the rod length does not lead to enhanced ability of creating excitons at the seed because of the reduced rod-to-seed exciton localization efficiency. This result confirms the existence of an optimal rod length for light-harvesting applications.

CONCLUSION

In conclusion, we have examined the mechanism of rod-to-seed exciton localization in CdSe@CdS dot-in-rod NR heterostructures with both type I and quasi-type II band alignments. We observed a universal rod length dependent exciton localization efficiency that decreased with the rod length (~75.7 ± 1.5% in a ~29 nm rod to 30.5 ± 2.6% in a 117 nm rod) and was independent of the CdSe/CdS band alignment. We showed that this universal length dependence could be reproduced by a model that accounted for the competition between ultrafast 1D exciton diffusion and ultrafast exciton trapping (τ_{Trap} = 0.78 ± 0.13 ps) on the CdS NR. Best fit to the measured results revealed an exciton diffusion constant of 2.3×10^{-4} m^2/s, which is slightly smaller than the reported value in bulk CdS. The proposed model can be used to predict the exciton localization efficiency in CdSe@CdS of any length and should be applicable to other NRs, providing a rational approach for optimizing NR morphologies for efficient yet cost-effective 1D heterostructure-based devices.

METHODS

CdSe@CdS NRs of varying dimensions were synthesized using approaches reported by Manna and co-workers,[16] with slight modifications.[58,59] CdSe QDs of different sizes were used as seeds, and the lengths and diameters of overcoated CdS NRs were controlled by the ratio of CdSe QD seeds to CdS NR precursors. Details can be found in the SI. Instruments for structural and optical characterizations of these CdSe@CdS NRs were also documented in the SI. Femtosecond transient absorption measurements were performed using laser lights from a regeneratively amplified Ti:sapphire laser system (Coherent Legend, 800 nm, 150 fs, 2.4 mJ/pulse, and 1 kHz repetition rate). Further details can be found in the SI.

Conflict of Interest: The authors declare no competing financial interest.

Supporting Information Available: Synthesis procedure, additional transient absorption spectra and kinetics, fitting procedures, and fitting parameters. This material is available free of charge *via* the Internet at http://pubs.acs.org.

Acknowledgment. T.L, J.P., and L.J.H. acknowledge the financial support from the U.S. Department of Energy, Office of Basic Energy Sciences, Solar Photochemistry Program (DE-FG02-12ER16347, DE-FG03-02ER15753)). J.R.M., N.P., and N.R. acknowledge funding by the National Science Foundation (CHE-1213758, DMR-0645618, DMR-130792). STEM and EDS images were acquired using an FEI Tecnai Osiris electron microscope supported by the National Science Foundation (EPS-1004083).

REFERENCES AND NOTES

1. Peng, X. G.; Manna, L.; Yang, W. D.; Wickham, J.; Scher, E.; Kadavanich, A.; Alivisatos, A. P. Shape Control of CdSe Nanocrystals. *Nature* **2000**, *404*, 59–61.
2. Milliron, D. J.; Hughes, S. M.; Cui, Y.; Manna, L.; Li, J.; Wang, L.-W.; Paul Alivisatos, A. Colloidal Nanocrystal Heterostructures with Linear and Branched Topology. *Nature* **2004**, *430*, 190–195.
3. Li, H.; Kanaras, A. G.; Manna, L. Colloidal Branched Semiconductor Nanocrystals: State of the Art and Perspectives. *Acc. Chem. Res.* **2013**, *46*, 1387–1396.
4. Shieh, F.; Saunders, A. E.; Korgel, B. A. General Shape Control of Colloidal CdS, CdSe, CdTe Quantum Rods and Quantum Rod Heterostructures. *J. Phys. Chem. B* **2005**, *109*, 8538–8542.

5. Giblin, J.; Kuno, M. Nanostructure Absorption: A Comparative Study of Nanowire and Colloidal Quantum Dot Absorption Cross Sections. *J. Phys. Chem. Lett.* **2010**, *1*, 3340–3348.
6. Giblin, J.; Syed, M.; Banning, M. T.; Kuno, M.; Hartland, G. Experimental Determination of Single CdSe Nanowire Absorption Cross Sections through Photothermal Imaging. *ACS Nano* **2010**, *4*, 358–364.
7. Carey, C. R.; LeBel, T.; Crisostomo, D.; Giblin, J.; Kuno, M.; Hartland, G. V. Imaging and Absolute Extinction Cross-Section Measurements of Nanorods and Nanowires through Polarization Modulation Microscopy. *J. Phys. Chem. C* **2010**, *114*, 16029–16036.
8. Manna, L.; Scher, E. C.; Li, L.-S.; Alivisatos, A. P. Epitaxial Growth and Photochemical Annealing of Graded CdS/ZnS Shells on Colloidal CdSe Nanorods. *J. Am. Chem. Soc.* **2002**, *124*, 7136–7145.
9. Mokari, T.; Banin, U. Synthesis and Properties of CdSe/ZnS Core/Shell Nanorods. *Chem. Mater.* **2003**, *15*, 3955–3960.
10. Htoon, H.; Hollingsworth, J. A.; Dickerson, R.; Klimov, V. I. Effect of Zero- to One-Dimensional Transformation on Multiparticle Auger Recombination in Semiconductor Quantum Rods. *Phys. Rev. Lett.* **2003**, *91*, 227401.
11. Htoon, H.; Hollingworth, J.; Malko, A.; Dickerson, R.; Klimov, V. Light Amplification in Semiconductor Nanocrystals: Quantum Rods *versus* Quantum Dots. *Appl. Phys. Lett.* **2003**, *82*, 4776.
12. Robel, I.; Bunker, B. A.; Kamat, P. V.; Kuno, M. Exciton Recombination Dynamics in CdSe Nanowires: Bimolecular to Three-Carrier Auger Kinetics. *Nano Lett.* **2006**, *6*, 1344–1349.
13. Zhu, H.; Lian, T. Enhanced Multiple Exciton Dissociation from CdSe Quantum Rods: The Effect of Nanocrystal Shape. *J. Am. Chem. Soc.* **2012**, *134*, 11289–11297.
14. Hu, J.; Li, L.-s.; Yang, W.; Manna, L.; Wang, L.-w.; Alivisatos, A. P. Linearly Polarized Emission from Colloidal Semiconductor Quantum Rods. *Science* **2001**, *292*, 2060–2063.
15. Talapin, D. V.; Koeppe, R.; Götzinger, S.; Kornowski, A.; Lupton, J. M.; Rogach, A. L.; Benson, O.; Feldmann, J.; Weller, H. Highly Emissive Colloidal CdSe/CdS Heterostructures of Mixed Dimensionality. *Nano Lett.* **2003**, *3*, 1677–1681.
16. Carbone, L.; Nobile, C.; De Giorgi, M.; Sala, F. D.; Morello, G.; Pompa, P.; Hytch, M.; Snoeck, E.; Fiore, A.; Franchini, I. R.; *et al.* Synthesis and Micrometer-Scale Assembly of Colloidal CdSe/CdS Nanorods Prepared by a Seeded Growth Approach. *Nano Lett.* **2007**, *7*, 2942–2950.
17. Hadar, I.; Hitin, G. B.; Sitt, A.; Faust, A.; Banin, U. Polarization Properties of Semiconductor Nanorod Heterostructures: From Single Particles to the Ensemble. *J. Phys. Chem. Lett.* **2013**, 502–507.
18. Sitt, A.; Salant, A.; Menagen, G.; Banin, U. Highly Emissive Nano Rod-in-Rod Heterostructures with Strong Linear Polarization. *Nano Lett.* **2011**, *11*, 2054–2060.
19. Wang, J.; Gudiksen, M. S.; Duan, X.; Cui, Y.; Lieber, C. M. Highly Polarized Photoluminescence and Photodetection from Single Indium Phosphide Nanowires. *Science* **2001**, *293*, 1455–1457.
20. Deka, S.; Quarta, A.; Lupo, M. G.; Falqui, A.; Boninelli, S.; Giannini, C.; Morello, G.; De Giorgi, M.; Lanzani, G.; Spinella, C.; *et al.* CdSe/CdS/ZnS Double Shell Nanorods with High Photoluminescence Efficiency and Their Exploitation as Biolabeling Probes. *J. Am. Chem. Soc.* **2009**, *131*, 2948–2958.
21. Pisanello, F.; Martiradonna, L.; Spinicelli, P.; Fiore, A.; Hermier, J. P.; Manna, L.; Cingolani, R.; Giacobino, E.; De Vittorio, M.; Bramati, A. Dots in Rods as Polarized Single Photon Sources. *Superlattices Microstruct.* **2010**, *47*, 165–169.
22. Kazes, M.; Lewis, D. Y.; Ebenstein, Y.; Mokari, T.; Banin, U. Lasing from Semiconductor Quantum Rods in a Cylindrical Microcavity. *Adv. Mater.* **2002**, *14*, 317–321.
23. Amirav, L.; Alivisatos, A. P. Photocatalytic Hydrogen Production with Tunable Nanorod Heterostructures. *J. Phys. Chem. Lett.* **2010**, *1*, 1051–1054.
24. Berr, M.; Vaneski, A.; Susha, A. S.; Rodriguez-Fernandez, J.; Doblinger, M.; Jackel, F.; Rogach, A. L.; Feldmann, J. Colloidal CdS Nanorods Decorated with Subnanometer Sized Pt Clusters for Photocatalytic Hydrogen Generation. *Appl. Phys. Lett.* **2010**, *97*, 0931081–0931083.
25. Brown, K. A.; Wilker, M. B.; Boehm, M.; Dukovic, G.; King, P. W. Characterization of Photochemical Processes for H2 Production by CdS Nanorod−[FeFe] Hydrogenase Complexes. *J. Am. Chem. Soc.* **2012**, *134*, 5627–5636.
26. Bang, J. U.; Lee, S. J.; Jang, J. S.; Choi, W.; Song, H. Geometric Effect of Single or Double Metal-Tipped CdSe Nanorods on Photocatalytic H2 Generation. *J. Phys. Chem. Lett.* **2012**, *3*, 3781–3785.
27. Khon, E.; Lambright, K.; Khnayzer, R. S.; Moroz, P.; Perera, D.; Butaeva, E.; Lambright, S.; Castellano, F. N.; Zamkov, M. Improving the Catalytic Activity of Semiconductor Nanocrystals through Selective Domain Etching. *Nano Lett.* **2013**, *13*, 2016–2023.
28. Xing, G.; Liao, Y.; Wu, X.; Chakrabortty, S.; Liu, X.; Yeow, E. K. L.; Chan, Y.; Sum, T. C. Ultralow Threshold Two-Photon Pumped Amplified Spontaneous Emission and Lasing from Seeded CdSe/CdS Nanorod Heterostructures. *ACS Nano* **2012**, *6*, 10835–10844.
29. Saba, M.; Minniberger, S.; Quochi, F.; Roither, J.; Marceddu, M.; Gocalinska, A.; Kovalenko, M. V.; Talapin, D. V.; Heiss, W.; Mura, A. Exciton-Exciton Interaction and Optical Gain in Colloidal CdSe/CdS Dot/Rod Nanocrystals. *Adv. Mater.* **2009**, *21*, 4942.
30. Reiss, P.; Protière, M.; Li, L. Core/Shell Semiconductor Nanocrystals. *Small* **2009**, *5*, 154–168.
31. Hines, M. A.; Guyot-Sionnest, P. Synthesis and Characterization of Strongly Luminescing ZnS-Capped CdSe Nanocrystals. *J. Phys. Chem.* **1996**, *100*, 468–471.
32. Dabbousi, B. O.; Rodriguez-Viejo, J.; Mikulec, F. V.; Heine, J. R.; Mattoussi, H.; Ober, R.; Jensen, K. F.; Bawendi, M. G. (CdSe)ZnS Core−Shell Quantum Dots: Synthesis and Characterization of a Size Series of Highly Luminescent Nanocrystallites. *J. Phys. Chem. B* **1997**, *101*, 9463–9475.
33. Peng, X.; Schlamp, M. C.; Kadavanich, A. V.; Alivisatos, A. P. Epitaxial Growth of Highly Luminescent CdSe/CdS Core/Shell Nanocrystals with Photostability and Electronic Accessibility. *J. Am. Chem. Soc.* **1997**, *119*, 7019–7029.
34. Scholes, G. D. Controlling the Optical Properties of Inorganic Nanoparticles. *Adv. Funct. Mater.* **2008**, *18*, 1157–1172.
35. Smith, A. M.; Nie, S. Semiconductor Nanocrystals: Structure, Properties, and Band Gap Engineering. *Acc. Chem. Res.* **2009**, *43*, 190–200.
36. Talapin, D. V.; Nelson, J. H.; Shevchenko, E. V.; Aloni, S.; Sadtler, B.; Alivisatos, A. P. Seeded Growth of Highly Luminescent CdSe/CdS Nanoheterostructures with Rod and Tetrapod Morphologies. *Nano Lett.* **2007**, *7*, 2951–2959.
37. Lupo, M. G.; Della Sala, F.; Carbone, L.; Zavelani-Rossi, M.; Fiore, A.; Lüer, L.; Polli, D.; Cingolani, R.; Manna, L.; Lanzani, G. Ultrafast Electron−Hole Dynamics in Core/Shell CdSe/CdS Dot/Rod Nanocrystals. *Nano Lett.* **2008**, *8*, 4582–4587.
38. Steiner, D.; Dorfs, D.; Banin, U.; Della Sala, F.; Manna, L.; Millo, O. Determination of Band Offsets in Heterostructured Colloidal Nanorods Using Scanning Tunneling Spectroscopy. *Nano Lett.* **2008**, *8*, 2954–2958.
39. Sitt, A.; Sala, F. D.; Menagen, G.; Banin, U. Multiexciton Engineering in Seeded Core/Shell Nanorods: Transfer from Type-I to Quasi-Type-II Regimes. *Nano Lett.* **2009**, *9*, 3470–3476.
40. Borys, N. J.; Walter, M. J.; Huang, J.; Talapin, D. V.; Lupton, J. M. The Role of Particle Morphology in Interfacial Energy Transfer in CdSe/CdS Heterostructure Nanocrystals. *Science* **2010**, *330*, 1371–1374.
41. Smith, E. R.; Luther, J. M.; Johnson, J. C. Ultrafast Electronic Delocalization in CdSe/CdS Quantum Rod Heterostructures. *Nano Lett.* **2011**, *11*, 4923–4931.
42. Kunneman, L. T.; Zanella, M.; Manna, L.; Siebbeles, L. D. A.; Schins, J. M. Mobility and Spatial Distribution of Photoexcited Electrons in CdSe/CdS Nanorods. *J. Phys. Chem. C* **2013**, *117*, 3146–3151.

43. Eshet, H.; Grünwald, M.; Rabani, E. The Electronic Structure of CdSe/CdS Core/Shell Seeded Nanorods: Type-I or Quasi-Type-II? *Nano Lett.* **2013**, *13*, 5880–5885.
44. She, C.; Demortière, A.; Shevchenko, E. V.; Pelton, M. Using Shape to Control Photoluminescence from CdSe/CdS Core/Shell Nanorods. *J. Phys. Chem. Lett.* **2011**, *2*, 1469–1475.
45. Rainò, G.; Stöferle, T.; Moreels, I.; Gomes, R.; Kamal, J. S.; Hens, Z.; Mahrt, R. F. Probing the Wave Function Delocalization in CdSe/CdS Dot-in-Rod Nanocrystals by Time- and Temperature-Resolved Spectroscopy. *ACS Nano* **2011**, *5*, 4031–4036.
46. Mauser, C.; Da Como, E.; Baldauf, J.; Rogach, A. L.; Huang, J.; Talapin, D. V.; Feldmann, J. Spatio-temporal Dynamics of Coupled Electrons and Holes in Nanosize CdSe-CdS Semiconductor Tetrapods. *Phys. Rev. B* **2010**, *82*, 0813061–0813064.
47. Lutich, A. A.; Mauser, C.; Da Como, E.; Huang, J.; Vaneski, A.; Talapin, D. V.; Rogach, A. L.; Feldmann, J. Multiexcitonic Dual Emission in CdSe/CdS Tetrapods and Nanorods. *Nano Lett.* **2010**, *10*, 4646–4650.
48. Luo, Y.; Wang, L.-W. Electronic Structures of the CdSe/CdS Core−Shell Nanorods. *ACS Nano* **2009**, *4*, 91–98.
49. Yoskovitz, E.; Menagen, G.; Sitt, A.; Lachman, E.; Banin, U. Nanoscale Near-Field Imaging of Excitons in Single Heterostructured Nanorods. *Nano Lett.* **2010**, *10*, 3068–3072.
50. Shabaev, A.; Efros, A. L. 1D Exciton Spectroscopy of Semiconductor Nanorods. *Nano Lett.* **2004**, *4*, 1821–1825.
51. Scholes, G. D.; Rumbles, G. Excitons in Nanoscale Systems. *Nat. Mater.* **2006**, *5*, 683–696.
52. Scholes, G. D.; Fleming, G. R.; Olaya-Castro, A.; van Grondelle, R. Lessons from Nature about Solar Light Harvesting. *Nat. Chem.* **2011**, *3*, 763–774.
53. Wu, K.; Chen, Z.; Lv, H.; Zhu, H.; Hill, C. L.; Lian, T. Hole Removal Rate Limits Photo-driven H2 Generation Efficiency in CdS-Pt and CdSe/CdS-Pt Semiconductor Nanorod-Metal tip Heterostructures. *J. Am. Chem. Soc.* **2014**, *136*, 7708–7716.
54. Bronstein, N. D.; Li, L.; Xu, L.; Yao, Y.; Ferry, V. E.; Alivisatos, A. P.; Nuzzo, R. G. Luminescent Solar Concentration with Semiconductor Nanorods and Transfer-Printed Micro-Silicon Solar Cells. *ACS Nano* **2013**, *8*, 44–53.
55. Kelestemur, Y.; Cihan, A. F.; Guzelturk, B.; Demir, H. V. Type-Tunable Amplified Spontaneous Emission from Core-Seeded CdSe/CdS Nanorods Controlled by Exciton-Exciton Interaction. *Nanoscale* **2014**, *6*, 8509–8514.
56. Wu, K.; Rodríguez-Córdoba, W. E.; Liu, Z.; Zhu, H.; Lian, T. Beyond Band Alignment: Hole Localization Driven Formation of Three Spatially Separated Long-Lived Exciton States in CdSe/CdS Nanorods. *ACS Nano* **2013**, *7*, 7173–7185.
57. She, C.; Bryant, G. W.; Demortière, A.; Shevchenko, E. V.; Pelton, M. Controlling the Spatial Location of Photoexcited Electrons in Semiconductor CdSe/CdS Core/Shell Nanorods. *Phys. Rev. B* **2013**, *87*, 155427.
58. Hill, L. J.; Richey, N. E.; Sung, Y.; Dirlam, P. T.; Griebel, J. J.; Lavoie-Higgins, E.; Shim, I.-B.; Pinna, N.; Willinger, M.-G.; Vogel, W.; Benkoski, J. J.; Char, K.; Pyun, J. Colloidal Polymers from Dipolar Assembly of Cobalt-Tipped CdSe@CdS Nanorods. *ACS Nano* **2014**, *8*, 3272–3284.
59. Hill, L. J.; Bull, M. M.; Sung, Y.; Simmonds, A. G.; Dirlam, P. T.; Richey, N. E.; DeRosa, S. E.; Shim, I.-B.; Guin, D.; Costanzo, P. J.; Pinna, N.; Willinger, M.-G.; Vogel, W.; Char, K.; Pyun, J. Directing the Deposition of Ferromagnetic Cobalt onto Pt-Tipped CdSe@CdS Nanorods: Synthetic and Mechanistic Insights. *ACS Nano* **2012**, *6*, 8632–8645.
60. Peter, Y. Y.; Cardona, M. *Fundamentals of Semiconductors: Physics and Materials Properties*; Springer: Berlin, 2010.
61. Lupo, M. G.; Zavelani-Rossi, M.; Fiore, A.; Polli, D.; Carbone, L.; Cingolani, R.; Manna, L.; Lanzani, G. Evidence of Electron Wave Function Delocalization in CdSe/CdS Asymmetric Nanocrystals. *Superlattices Microstruct.* **2010**, *47*, 170–173.
62. Klimov, V. I. Optical Nonlinearities and Ultrafast Carrier Dynamics in Semiconductor Nanocrystals. *J. Phys. Chem. B* **2000**, *104*, 6112–6123.
63. Wu, K.; Zhu, H.; Liu, Z.; Rodríguez-Córdoba, W.; Lian, T. Ultrafast Charge Separation and Long-Lived Charge Separated State in Photocatalytic CdS−Pt Nanorod Heterostructures. *J. Am. Chem. Soc.* **2012**, *134*, 10337–10340.
64. Wei, H. H.-Y.; Evans, C. M.; Swartz, B. D.; Neukirch, A. J.; Young, J.; Prezhdo, O. V.; Krauss, T. D. Colloidal Semiconductor Quantum Dots with Tunable Surface Composition. *Nano Lett.* **2012**, *12*, 4465–4471.
65. Wu, K.; Rodríguez-Córdoba, W.; Lian, T. Exciton Localization and Dissociation Dynamics in CdS and CdS−Pt Quantum Confined Nanorods: Effect of Nonuniform Rod Diameters. *J. Phys. Chem. B* **2014**, *118*, 14062–14069.
66. Stryer, L. Fluorescence Energy Transfer as a Spectroscopic Ruler. *Annu. Rev. Biochem.* **1978**, *47*, 819–846.
67. Van Zeghbroeck, B. *Principles of Semiconductor Devices*; Colarado University, 2004.
68. Warman, J. M.; De Haas, M. P.; Van Hovell tot Westerflier, S. W. F. M.; Binsma, J. J. M.; Kolar, Z. I. Electronic Processes in Semiconductor Materials Studied by Nanosecond Time-Resolved Microwave Conductivity. 1. Cadmium Sulfide Macroscopic Crystal. *J. Phys. Chem.* **1989**, *93*, 5895–5899.
69. Islam, M. N.; Woods, J. The Effect of Crystal Inhomogeneity on the Threshold Field for Current Saturation in Photoconducting CdS. *J. Phys. D: Appl. Phys.* **1970**, *3*, 1297.
70. Spear, W. E.; Mort, J. Electron and Hole Transport in CdS Crystals. *Proc. Phys. Soc.* **1963**, *81*, 130.
71. Mort, J.; Spear, W. E. Hole Drift Mobility and Lifetime in CdS Crystals. *Phys. Rev. Lett.* **1962**, *8*, 314–315.
72. Islam, M. N.; Woods, J. Acoustoelectric Interaction and the Drift Mobility of Holes in CdS. *Solid State Commun.* **1969**, *7*, 1457–1461.
73. Khandros, L. I.; Pekar, G. S.; Sheinkman, M. K.; Shtrum, E. L. High-Temperature Investigations of CdS Single Crystals. I. Electron Concentration, Cd Solubility, and Charge of Intrinsic Defects. *Phys. Status Solidi A* **1976**, *33*, 765–771.
74. Houston, P. L. *Chemical Kinetics and Reaction Dynamics*; Courier Dover Publications, 2012.
75. Joyce, H. J.; Wong-Leung, J.; Yong, C.-K.; Docherty, C. J.; Paiman, S.; Gao, Q.; Tan, H. H.; Jagadish, C.; Lloyd-Hughes, J.; Herz, L. M.; Johnston, M. B. Ultralow Surface Recombination Velocity in InP Nanowires Probed by Terahertz Spectroscopy. *Nano Lett.* **2012**, *12*, 5325–5330.